Contribution from the Department of Chemistry, Western Washington University, Bellingham, Washington 98225, Department of Chemistry, University of Notre Dame, Notre Dame, Indiana 46556, and Institut für Anorganische Chemie, Technische Hochschule Darmstadt, D-6100 Darmstadt, West Germany

Metal Complexes with Tetrapyrrole Ligands. 49.[1] Solid-State and Solution Structures of Iron(III) Porphodimethenes. Effects of Steric Hindrance

Andreas Botulinski,[2a] Johann W. Buchler,*[2a] Young J. Lee,[2b] W. Robert Scheidt,[2b] and Mark Wicholas*[2c]

Received September 24, 1987

Two square-pyramidal iron(III) 5,15-dialkyloctaethylporphodimethenes, $Fe(OEPR_2)Cl$ (R = CH_3, $C(CH_3)_3$), have been synthesized, and their H NMR spectra have been interpreted. Variable-temperature magnetic susceptibility measurements suggest a $S = {}^5/_2$ ground state with a zero-field splitting parameter, $D = 15$ cm^{-1}. The isotropic shifts are shown to have substantial contact and dipolar contributions, whereas the nuclear relaxation rates, T_2, and resulting line widths appear to be dipolar in origin. The solution stereochemistry of these complexes is resolved from a comparison of relative ^{1}H NMR line widths: the apical ligand, chloride, binds syn axial in $Fe(OEPMe_2)Cl$ but anti axial in $Fe(OEPBu_2)Cl$. A single-crystal X-ray structural determination of $Fe(OEPMe_2)Cl$ is reported. Crystals are monoclinic, space group $C2/c$, $Z = 4$, with $a = 15.829$ (3) Å, $b = 15.909$ (3) Å, $c = 14.794$ (2) Å, and $\beta = 113.16$ (1)°. A full-matrix least-squares refinement yielded $R = 0.038$ with the use of 2681 independent reflections. The coordination geometry is square pyramidal with Cl^- in the syn-axial, apical position, 2.229 (1) Å distant from Fe. The average Fe–N bond length is 2.066 Å.

Introduction

The synthesis and structural elucidation of metalloporphodimethene complexes has been of major concern to us for some years.[3-6] The porphodimethenes are a class of reduced porphyrins (5,15-dihydroporphyrins) in which hydrogenation has occurred at two opposite meso carbons. Our interest has been in the 5,15-dialkylporphodimethenes, $H_2(OEPR_2)$, which are derived from octaethylporphyrin H_2OEP by the following sequence of reactions: reduction of Zn(OEP) with sodium anthracenide, alkylation with alkyl halide, demetalation with acetic acid, and isolation of the neutral macrocycle having both R groups axial

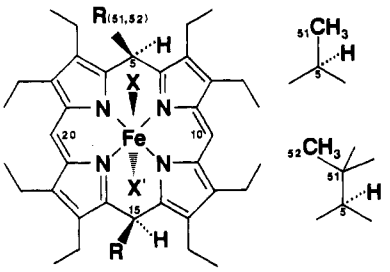

1: $Fe(OEpMe_2)Cl$ (R = CH_3, X = Cl, no X′)
2: $Fe(OEPBu_2)Cl$ (R = $C(CH_3)_3$; X′ = Cl, no X)

which is the most stable of the three possible stereoisomers.[7]

The 5,15-dialkylporphodimethenes, like the related porphyrins, are excellent tetrapyrrole ligands and readily insert divalent and trivalent metal ions.[8] The metalloporphodimethenes in some respects, however, have noticeably different properties when compared to the metalloporphyrins, and this is a consequence of reductive alkylation at the meso carbon positions (5,15-C). Metalloporphodimethenes, for example, are distinctly nonplanar with folding of the macrocycle along the 5,15-C bond axis and ruffling of the individual pyrrole rings.[9] Also the greatly diminished aromaticity of the porphodimethene is evident from the ^{1}H NMR spectra, as for example with the diamagnetic nickel(II) porphodimethenes.[5] Finally the 5,15-dialkylporphodimethenes, having three possible stereoisomers, present an added degree of complexity not found in simple porphyrin systems.

In our previous studies we described the synthesis and ^{1}H NMR spectra of the diamagnetic nickel(II) and paramagnetic cobalt(II) 5,15-dialkylporphodimethenes.[4,5] In the latter case, analysis of relative line widths and isotropic shifts was useful in detailing the conformation of these complexes in solution. We have now extended our NMR study of paramagnetic 5,15-dialkylporphodimethenes to the $S = {}^5/_2$ iron(III) 5,15-dialkylporphodimethenes of formula $Fe(OEPR_2)Cl$, a class of compounds that we briefly described in a prior communication.[10,11] Our focus is on stereochemistry and specifically that information about the geometry of paramagnetic species in solution which can be extracted from a study of ^{1}H NMR isotropic shifts and line widths.

We also report the solid-state molecular structure of $Fe(OEPMe_2)Cl$ as determined by single-crystal X-ray diffraction, and this is compared with our conclusions from the ^{1}H NMR solution spectrum.

Experimental Section

Synthesis of (5,15-Dialkyl-5,15-dihydro-2,3,7,8,12,13,17,18-octaethylporphyrinato)iron(III) Complexes. $Fe(OEPMe_2)Cl$ (1). This was prepared from the parent porphodimethene as described previously.[11] Crystals suitable for X-ray data collection were obtained from dichloromethane.

$Fe(OEPBu_2)Cl$ (2). A solution of 74 mg (0.1 mmol) of hydroxoiron(III) porphodimethene, $Fe(OEPBu_2)OH$,[3,10] in 50 mL of dichloromethane was refluxed for 15 min with 2 mL of aqueous hydrochloric acid (18%). After separation of the aqueous layer, the organic layer was evaporated in vacuo and the residue recrystallized from dichloromethane. Drying in vacuo at 40°C gave 61.3 mg (84%) of a black-brown powder. Recrystallization from *n*-decane produced bushes of very small, dark brown crystals.

Anal. Calcd for $C_{44}H_{62}N_4ClFe$ (mol wt 738.30): C, 71.58; H, 8.47; N, 7.59; Fe, 7.56; Cl, 4.80. Found. C, 70.50; H, 8.36; N, 7.39. IR

(1) Part 48: Buchler, J. W.; Dreher, C.; Herget, G. *Liebigs Ann. Chem.*, in press.
(2) (a) Technische Hochschule Darmstadt. (b) University of Notre Dame. (c) Western Washington University.
(3) Buchler, J. W.; Lay, K. L.; Lee, Y. L.; Scheidt, W. R. *Angew. Chem.* **1982**, *94*, 456; *Angew. Chem. Suppl.* **1982**, 996; *Angew. Chem., Int. Ed. Engl.* **1982**, *21*, 432.
(4) Botulinski, A.; Buchler, J. W.; Tonn, B.; Wicholas, M. *Inorg. Chem.* **1985**, *20*, 3239.
(5) Botulinski, A.; Buchler, J. W.; Wicholas, M. *Inorg. Chem.* **1987**, *26*, 1540.
(6) Botulinski, A.; Buchler, J. W.; Abbes, N. E.; Scheidt, W. R. *Liebigs Ann. Chem.* **1987**, 305.
(7) Botulinski, A.; Buchler, J. W.; Lay, K. L.; Stoppa, H. *Liebigs Ann. Chem.* **1984**, 1259.
(8) (a) Buchler, J. W.; Puppe, L.; Schneehage, H. H. *Justus Liebigs Ann. Chem.* **1971**, *749*, 134. (b) Buchler, J. W.; Puppe, L. *Justus Liebigs Ann. Chem.* **1974**, 1046. (c) Botulinski, A. Diplomarbeit, Technische Hochschule Darmstadt, 1981.
(9) Dwyer, P. N.; Buchler, J. W.; Scheidt, W. R. *Inorg. Chem.* **1974**, *96*, 2789.
(10) Botulinski, A.; Buchler, J. W.; Lay, K. L.; Ensling, J.; Twilfer, H.; Billecke, J.; Leuken, H.; Tonn, B. *Adv. Chem. Ser.* **1982**, *No. 201*, 253.
(11) Buchler, J. W.; Lay, K. L. *Z. Naturforsch., B: Anorg. Chem., Org. Chem.* **1975**, *30B*, 385.

0020-1669/88/1327-0927$01.50/0

(KBr): 1605, 1214, 1005, 865 cm^{-1} (porphodimethene bands). IR (CsI): 349 cm^{-1} (FeCl); bands for OH (3630 cm^{-1}) or FeOR (590 cm^{-1}) were absent. UV/vis (CH_2Cl_2): λ_{max} (log ϵ) = 407 (4.64), 451 (4.42, shoulder), 632 nm (3.51, shoulder). On attempted alumina chromatography, the compound hydrolyzes to $Fe(OEPBu_2)OH$.

Magnetic Resonance and Susceptibility. The ^1H NMR spectra were measured on Bruker 300- and 500-MHz instruments. All chemical shifts are reported relative to Me_4Si. The isotropic shifts in $CDCl_3$ are relative to $Al(OEPMe_2)OMe$ for **1** and to $Al(OEPBu_2)OH$ for **2**. Most spectra were collected with use of 32K data points, a 14 μs-pulse, and a delay time of 2 s. Under these conditions no saturation of signal occurred. Line widths, $\Delta\nu_{1/2}$, were measured at half-height of the NMR signal. Deuteriated solvents were purchased from Merck and used without further purification. Magnetic susceptibilities were measured by the Faraday method as described previously.[12]

Crystallographic Study. Dark brown crystals of $Fe(OEPMe_2)Cl$ were obtained from a dichloromethane solution. Preliminary examination and data collection were performed with Mo Kα radiation on an Enraf-Nonius CAD4 computer-controlled K-axis diffractometer equipped with a graphite-crystal incident beam monochromator. A preliminary X-ray study established a monoclinic four-molecule unit cell with *Cc* or *C2/c* as the possible space groups. Lattice constants a = 15.829 (3) Å, b = 15.909 (3) Å, c = 14.794 (2) Å, and β = 113.16 (1)° (λ = 0.71073 Å) were obtained from least-squares refinement by using the setting angles of 25 reflections in the range $25.9 < 2\theta < 28.8°$, measured by the computer-controlled diagonal slit method of centering. There were $12 \pm 2\theta$ pairs. These constants led to a calculated density at 20 ± 1 °C of 1.27 g/cm^3 for a cell content of $4FeClN_4C_{38}H_{50}$; the observed density (by flotation) is 1.27 g/cm^3.

Intensity data were collected at room temperature by using the θ–2θ scan technique. The scan rate was 4.12 deg/min (2θ), and the scan range was calculated as follows: ω scan width = 0.80 + 0.35 tan θ. The dimensions of the crystal used in data collection were 0.10 × 0.20 × 0.70 mm. A total of 8402 reflections ($0 < h < 21$, $-21 < k < 21$, and $-19 < l < 19$) were collected for the monoclinic lattice, $4.0 < 2\theta < 54.90°$. Intensities of equivalent reflections were averaged, and 4343 were unique. The merging R value (on I) was 0.021. Four standard reflections were measured every 1 h of X-ray exposure, and no crystal decomposition was noted. With a linear absorption coefficient of 0.548 mm^{-1} and relative transmission variations of <±3%, no absorption correction was made. All data having $F_o < \sigma(F_o)$ were taken to be unobserved; 2681 independent data were considered observed (68.5% of the theoretical number possible). Only the observed data were used for the refinement of structure.

The structure was solved by Patterson synthesis and the direct-methods program DIRDIF.[13] This program was used because the iron atom was located on the special position along the twofold axis of symmetry. At this stage, the structure was confirmed to be isomorphous with $TiO(OEPMe_2)$ of space group $C2/c$.[14] Full-matrix least-squares refinement was followed by a difference Fourier synthesis, which revealed electron density concentrations appropriately located for the hydrogen atoms. Hydrogen atoms were located and their positions and isotropic thermal parameters were refined with the limited shift of 0.25. The refinement was then carried to convergence of all heavy atoms with anisotropic thermal parameters. The final value of $R_1 = [F_o - F_c]/\sum F_o$ was 0.038; that of $R_2 = [\sum w(F_o - F_c)^2/\sum w(F_o)^2]^{1/2}$ was 0.048. The estimated standard deviation of an observation of unit weight was 1.45. The final parameter shifts of heavy atoms were less than 10% of the estimated standard deviations except those for C(12) and C(32) (shift/error = 0.37, 0.32 respectively). The final difference Fourier map showed no significant residual electron density. The highest peak in the final difference Fourier had a height of 0.42 e/Å^3 and the others are less than 0.26 e/Å^3. The highest peaks were around the iron atom.

(12) Merz, L. Doctoral Dissertation, Technische Hochschule Darmstadt, 1979.

(13) DIRDEF: Beurskens, P. T.; Bosman, W. P.; Doesbury, H. M.; Gould, R. O.; van den Hark, Th. E. M.; Prick, P. A. J.; Noordik, J. H.; Stempel, M.; Smits, J. M. M. Technical Report 1984/1; Crystallography Laboratory: Toernooiveld, 6525 Ed Nijmegen, The Netherlands. Other programs used in this study included local modifications of Jacobson's ALLS, Zalkin's FORDAP, Busing and Levy's ORFFE and ORFLS, and Johnson's ORTEP2. Atomic form factors were from: Cromer, D. T.; Mann, J. B. *Acta Crystallogr., Sect. A: Cryst. Phys. Diffr., Theor. Gen. Crystallogr.* **1968**, *A24*, 321. Real and imaginary corrections for anomalous dispersion in the form factor of the iron and chlorine atoms were from: Cromer, D. T.; Liberman, D. J. *J. Chem. Phys.* **1970**, *53*, 1891. Scattering factors for hydrogens were from: Stewart, R. F.; Davidson, E. R.; Simpson, W. T. *Ibid.* **1965**, *42*, 3175. All calculations were performed on a VAX 11/730.

(14) Dwyer, P. N.; Puppe, L.; Buchler, J. W.; Scheidt, W. R. *Inorg. Chem.* **1975**, *14*, 1782.

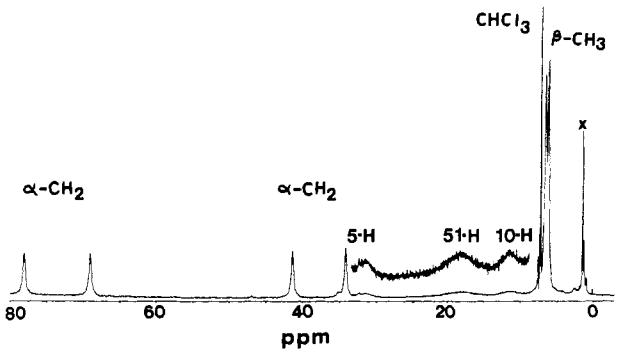

Figure 1. Proton NMR spectrum of $Fe(OEPMe_2)Cl$ (**1**) in $CDCl_3$ at 293 K (× denotes impurity).

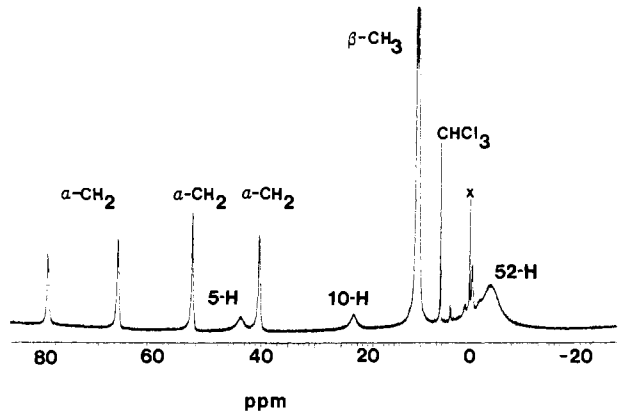

Figure 2. Proton NMR spectrum of $Fe(OEPBu_2)Cl$ (**2**) in $CDCl_3$ at 223 K (× denotes impurity).

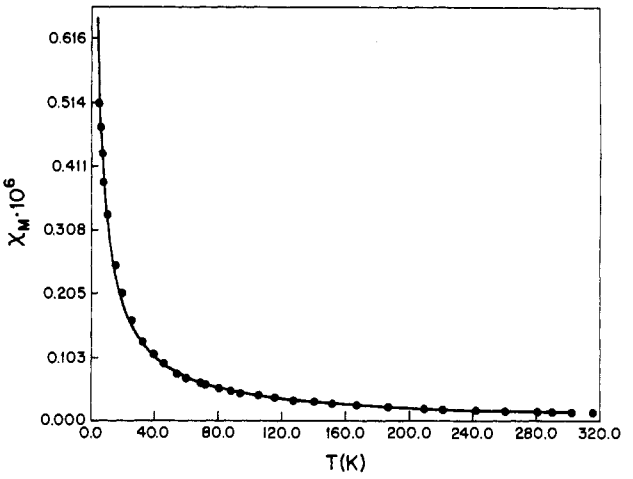

Figure 3. Magnetic susceptibility vs temperature curve for $Fe(OEPBu_2)Cl$ (**2**). The solid line represents the best data fit.

Results and Discussion

Iron(III) 5,15-dialkylporphodimethenes can be synthesized by the reaction of $Fe(CO)_5$ with metal-free dialkylporphodimethene in the presence of the oxidizing agent I_2.[11] The two complexes discussed herein, $Fe(OEPMe_2)Cl$ (**1**) and $Fe(OEPBu_2)Cl$ (*2*), were prepared respectively by acidification of the intermediates $Fe(OEPBu_2)OH$ and $[Fe(OEPMe_2)]_2O$ with aqueous HCl (see Experimental Section). Both products have been characterized completely by elemental analysis and UV/vis, IR, and ^1H NMR spectroscopy.

The very broad and strongly shifted ^1H NMR signals (Figures 1 and 2) are suggestive of an $S = {}^5/_2$ ground state for these molecules; however, to establish this unequivocally and thereby eliminate the possibility of a spin-admixed $S = {}^3/_2, {}^5/_2$ ground state, the solid-state magnetic susceptibility of $Fe(OEPBu_2)Cl$ was measured from 5 to 316 K. The magnetic moment at room

temperature is 5.85 μ_B and remains essentially constant to 40 K at which point it drops steadily to a value of 4.6 at 5.1 K. The susceptibilities were fit to an axial Hamiltonian[15] for monomeric $S = {}^5/_2$ iron(III) of the form

$$H = D[S_z^2 - S(S+1)] + g\beta\vec{H}\cdot\vec{S}$$

and the best results were obtained for $g_\parallel = g_\perp = 2.0$ and $D = 15.0\ cm^{-1}$ by using the computer program STEPT.[16] The experimental data points and the computer-generated plot are illustrated in Figure 3. The closeness of fit indicates a pure $S = {}^5/_2$ ground state. This is also consistent with magnetic susceptibility results for the closely related, square-pyramidal, $S = {}^5/_2$, iron(III) porphyrin halides.[17]

In what follows, the ^1H NMR spectra of the chloroiron(III) 5,15-dialkylporphodimethenes shall be interpreted by assuming an $S = {}^5/_2$ ground state and approximate tetragonal symmetry. The NMR spectra of paramagnetic species, in the best of circumstances, may contain information relevant to metal–ligand bonding and the molecular geometry in solution. Both isotropic shifts and relative line widths are of importance. The isotropic shift $(\Delta H/H)_{iso}$ is defined as the sum of two components[18]

$$(\Delta H/H)_{iso} = (\Delta H/H)_{con} + (\Delta H/H)_{dip} \quad (1)$$

The contact shift, $(\Delta H/H)_{con}$, is directly related to the spin density at the ^1H nucleus resulting from spin delocalization via covalency, whereas the dipolar shift, $(\Delta H/H)_{dip}$, results from a dipolar, through-space interaction and is related to the magnetic anisotropy, the zero-field splitting, and the molecular geometry.

The contact term in a $S = {}^5/_2$ system with tetragonal symmetry is

$$\left(\frac{\Delta H}{H}\right)_{con} = \left(\frac{A}{\hbar}\right)\frac{35g\beta}{12\gamma_N kT}\left[1 - \frac{32(g_\parallel - g_\perp)D}{45gkT}\right] \quad (2)$$

where $A/\hbar$ is the electron spin-nuclear spin hyperfine coupling constant in rad s^{-1} and the other symbols have their normal meanings.[18] Since the magnetic susceptibility measurements for **2** are best fit with an isotropic **g** tensor, we assume that the T^{-2} term in (2) is negligible.

The dipolar shift for a proton in an $S = {}^5/_2$ system is given as[18]

$$\left(\frac{\Delta H}{H}\right)_{dip} = \frac{35\beta^2(g_\parallel^2 - g_\perp^2)(3\cos^2\theta - 1)}{36kTr^3} \times \left[1 - \frac{32\left(g_\parallel^2 + \frac{1}{2}g_\perp^2\right)D}{15(g_\parallel^2 - g_\perp^2)kT}\right] \quad (3)$$

where r is the proton–metal distance and θ is the angle which the vector $\vec{r}$ makes with the tetragonal axis. The term $(3\cos^2\theta - 1)/r^3$ is often called the geometric factor, G. When the **g** tensor is isotropic, (3) reduces to

$$\left(\frac{\Delta H}{H}\right)_{dip} = -\frac{28g^2\beta^2DG}{9(kT)^2} \quad (4)$$

NMR line widths can provide additional information about the geometry of paramagnetic molecules in solution. The line width, $\Delta\nu_{1/2}$, is related to the transverse relaxation time, T_2, as follows: $\pi\Delta\nu_{1/2} = T_2^{-1}$. Nuclear relaxation occurs predominantly via dipolar coupling of the nuclear and electronic magnetic moments, and for electronic states uncomplicated by large zero-field splitting, T_2^{-1} is given by the Solomon–Bloembergen equation (eq 5), where

$$T_2^{-1} = \frac{\gamma_N g^2\beta^2 S(S+1)}{15r^6}\left(7\tau_c + \frac{13\tau_c}{1 + \omega_s^2\tau_c^2}\right) \quad (5)$$

τ_c represents the correlation time for the dipolar interaction and ω_s is the frequency of the electron spin transition.[19] With large zero-field splitting, as is the case here, the bracketed term of the Solomon–Bloembergen equation is no longer valid although the $1/r^6$ proportionality should still be operative since it is an invariant property of dipolar coupling. The relative line widths should still be useful as measures of relative proton–metal distances assuming that nuclear relaxation is dominated by a dipolar coupling mechanism. We shall define a line-width factor $L = 10^3/r^6$ and use the relationship $L_i/L_j = (\Delta\nu_{1/2})_i/(\Delta\nu_{1/2})_j$ for protons i and j.

The analysis of the NMR spectra, both isotropic shifts and line widths, is carried out in a fashion similar to that described previously for the cobalt(II) 5,15-dialkylporphodimethenes:[4] that is, a trial structure, based upon the crystal structure of Fe(OEPBu$_2$)OH,[3] is chosen and varied in order to assess the change in geometry upon the calculated geometric factors and line-width factors. These factors are calculated for all protons except β-CH_3. When bond rotation occurs, they are calculated by computer for 1° rotation intervals and then averaged. The objective is to deduce a structure for Fe(OEPR$_2$)Cl in solution that is consistent with the NMR spectra and specifically to determine whether Cl^- coordinates from the top side (syn axial) or bottom side (anti axial). The coordination site of chloride (top or bottom) has a major effect on the NMR spectrum of Fe(OEPR$_2$)Cl because of the axial asymmetry of the dialkylporphodimethene. In square-pyramidal complexes the metal ion is displaced substantially out of the coordination plane. For Fe(OEPBu$_2$)OH, for example, in which hydroxide coordinates anti axial, the metal displacement is 0.40 Å below the tetraaza plane.[3] The 5,15-dialkylporphodimethenes are distinctly nonplanar ligands, and because of the folding and ruffling mentioned previously, 5-H lies above and 10-H lies below the tetraaza plane. When chloride coordinates from the top, the iron(III) becomes closer to 5-H and 51-H (or 52-H), and simultaneously more distant from 10-H. This pattern is reversed if coordination of chloride occurs from the bottom. Since $\Delta\nu_{1/2} \propto 1/r^6$, these two stereoisomers can be distinguished from one another on the basis of relative line widths.

Fe(OEPBu$_2$)Cl. The NMR spectrum of Fe(OEPBu$_2$)Cl (**2**) (Figure 2) is discussed first because there is less ambiguity in its interpretation. There are two sets of α-CH_2 protons, each set being diastereotopic and anisochronous, two sets of β-CH_3 protons, and one set each of 5,15-H, 10,20-H, and 52-H protons. Assignments are straightforward save for the 5,15-H and 10,20-H resonances, which are identified from line widths and dipolar shift calculations (vide infra). Chemical shifts, isotropic shifts, and line widths are listed in Table I together with those of **1**.

As a working model for the calculation of geometric and linewidth factors, we assume that Cl^- coordinates anti axial. In fact it is very unlikely that chloride could coordinate syn axial and fit into the pocket between the two *tert*-butyl groups. In this model the iron is placed 0.40 Å below the coordination plane and 2.04 Å from the pyrrole nitrogens. Normal pyrrole ring bond distances and angles are chosen based upon known crystallographic data, and a 40° dihedral roof angle and 12° ruffling of the pyrrole rings are used. Finally, to connect the pyrrole rings properly, the 5,15-C atoms are placed 3.35 Å from the ring center and 0.66 Å above the tetraaza plane, while the 10,20-C atoms are positioned 3.31 Å from the ring center and 0.60 Å below the tetraaza plane. The two signals in question, those of 5,15-H and 10,20-H, are at 25.0 and 11.8 ppm, and the relative line widths are approximately 1.20/1 with the upfield resonance being broader. For this model geometry and all reasonable perturbations thereof, we calculate that 10,20-H should be closer to iron than 5,15-H and

(15) An axial Hamiltonian was chosen since the EPR spectrum of **2** in a toluene glass at 77K is axial with $g_\perp = 5.83$ and $g_\parallel = 2.00$ for the transition associated with the lowest Kramers' doublet.[10]

(16) Hodges, K. D.; Wollman, R. G.; Barefield, E. K.; Hendrickson, D. N. *Inorg. Chem.* **1977**, *16*, 2746.
(17) Behere, D. V.; Birdy, R.; Mitra, S. *Inorg. Chem.* **1982**, *21*, 386.
(18) Bertini, I.; Luchinat, C. *NMR of Paramagnetic Molecules in Biological Systems*; Benjamin/Cummings: Menlo Park, CA, 1986; Chapter 2.

(19) See ref 18; Chapter 3.

Table I. ^{1}H NMR Chemical Shifts (ppm),[a] Isotropic Shifts (ppm),[b] and Line Widths (Hz)[c] for Fe(OEPR$_2$)Cl in $CDCl_3$ at 293 K

	proton					
compd	5-H	10-H	α-CH_2	β-CH_3	51-H	52-H
Fe(OEPMe$_2$)Cl (**1**)	*31.4*	*11.0*	*78.1, 69.1*	*6.4, 6.0*	*18.7*	···
			41.3, 34.2			
	26.9	4.0	75.5, 66.5	5.2, 4.8	16.9	
			38.7, 31.6			
	(630)	(630)	(110–130)		(1240)	
Fe(OEPBu$_2$)Cl (**2**)	*25.0*	*11.8*	*66.4, 41.7*	*8.39, 7.67*	···	1.2
			60.7, 40.2			
	21.0	4.9	63.8, 39.1	7.21, 6.49	···	0.1
			58.1, 37.6			
	(380)	(460)	(62–76)	(58)		(1190)

[a] The chemical shifts are listed in italics and are relative to Me_4Si. [b] Isotropic shifts for **1** are relative to Al(OEPMe$_2$)OMe[8c] and for **2** are relative to Al(OEPBu$_2$)OH.[8c] [c] The line width is given in parentheses. Linewidths were measured at 500 MHz for **1** and at 300 MHz for **2**.

Table II. Line Width Factors for Fe(OEPR$_2$)Cl

proton	$\langle r \rangle$, Å	$\langle L \rangle$[a]	$\Delta\nu_{1/2}$,[b] Hz
	Fe(OEPMe$_2$)Cl		
5-H	4.31	12.7	10.0
10-H	4.48	10.0	10.0
51-H	4.25	19.7	21.4
α-CH_2	5.97	1.80	1.7–2.1
	6.01	1.72	
	Fe(OEPBu$_2$)Cl		
5-H	4.46	10.0	10.0
10-H	4.29	12.6	12.1
52-H	4.81	30.9	31.3
α-CH_2	5.97	1.80	1.6–2.0
	6.01	1.72	

[a] All values are relative to 10.0 for 10-H in **1** and 10.0 for 5-H in **2**. [b] All values are relative to 10.0 for 5-H.

Table III. Geometric Factors, Dipolar Shifts, and Contact Shifts for Fe(OEPMe$_2$)Cl and Fe(OEPBu$_2$)Cl

proton	$\langle G \rangle$, Å^{-3}	$(\Delta H/H)_{dip}$,[a] ppm	$(\Delta H/H)_{con}$, ppm
	Fe(OEPMe$_2$)Cl		
5-H	−0.0124	24.2	2.7
10-H	−0.0118	23.0	−19.0
51-H	−0.000373	0.7	16.2
α-CH_2	−0.00429	8.5	67.0, 58.0
	−0.00442	8.5	30.2, 23.1
	Fe(OEPBu$_2$)Cl		
5-H	−0.00998	19.5	1.5
10-H	−0.0118	23.0	−18.1
52-H	0.0115	−22.4	22.5
α-CH_2	−0.00429	8.5	55.3, 49.6
	−0.00442	8.5	30.6, 29.1

[a] Dipolar shifts are calculated from (4) by using D = 15 cm^{-1}.

hence that the 10,20-H resonance should be broader. On this basis, the upfield resonance of the pair is assigned to 10,20-H. The calculated proton–metal distances and line-width factors for these and all protons based upon the model geometry are listed in Table II.

There are four α-CH_2 resonances belonging to the two sets of geminal protons. We assume that the two low-field resonances constitute one pair and that the two high-field resonances constitute a second pair. On the basis of this assignment, the spread between each pair, 5.7 and 1.5 ppm, respectively, at 293 K, is comparable to the spread of 3.6 ppm reported for Fe(OEP)Cl in CD_2Cl_2.[20]

The *tert*-butyl proton resonance is the broadest in the NMR spectrum, even though 52-H is more distant from iron than 5,15-H or 10,20-H. This is readily explained by the model line-width calculations. Assuming free rotation of the *ter*-butyl group, we calculate that the 52-H protons can move as close as 2.3 Å to iron. At this short distance $1/r^6$ makes a disproportionately large contribution to $\langle L \rangle$, hence the very broad signal. A similarly broad NMR signal for the 52-H resonance was observed in Co(OEP-Bu$_2$).[4]

Collectively there is very good agreement between the calculated values of $\langle L \rangle$ and the observed relative line widths, thus suggesting that our geometrical model with anti-axial coordination of chloride is correct. The model geometry proposed above should not, however, be construed as the *true* geometry of **2**, but rather one of a set of closely related structures that would present a reasonable correspondence between relative line widths and calculated line-width factors. On the other hand, were syn-axial coordination of chloride to occur, we calculate that the *tert*-butyl proton line width would increase to 3000 Hz because of the proximity of iron to 52-H.

The dipolar and contact shifts are calculated via (4) and (1), respectively, with D = 15 cm^{-1}, and the geometric factors are computed on the basis of the model geometry. The values of $\langle G \rangle$, $(\Delta H/H)_{dip}$, and $(\Delta H/H)_{con}$ are listed in Table III. The large, positive contact shift for 52-H—too large for σ-delocalization through the macrocycle—results from direct overlap of the appropriate half-filled d orbital (d_{xz}, d_{yz}) with 52-H as it closely approaches Fe(III).

The proposed upfield contact shift for 10-H is a sign of unpaired spin delocalization via π-type spin polarization.[18] The remaining contact shifts, all downfield, while readily consistent with σ-delocalization, do not preclude the possibility of simultaneous π-delocalization. Comparisons can be made with two previously studied, related systems: the more highly conjugated metalloporphyrins and the very similar metallopyrromethenes. Isotropic shifts for Fe(OEP)Cl have been reported,[21] and the meso proton resonance, comparable to 10,20-H, is shifted strongly upfield: $(\Delta H/H)_{iso}$ = −65.1 ppm. The contact shift, estimated as −80.4 ppm, was attributed to d_π–p_π* delocalization involving the lowest empty π* orbital of OEP.[22] The pyrromethene ligand

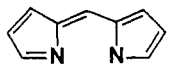

is equivalent to a half-porphodimethene with the meso position of the former being equivalent to the 10,20-H position of the latter. The upfield meso proton contact shifts observed in the ^{1}H NMR spectra of the nickel(II) and cobalt(II) pyrromethene chelates, were attributed by Eaton and La Lancette[22] to spin delocalization into the lowest empty ligand π* orbital, a conclusion supported by a Hückel π molecular orbital calculation.

Since porphodimethenes are nonplanar ligands, there is no separability of σ from π as is the case in porphyrins and pyrromethenes. However the lowest unoccupied ligand molecular orbital probably bears some correspondence to a π* orbital, i.e., large coefficients for p_π atomic orbitals orthogonal to the C-H bonds, and it is delocalization into this molecular orbital that causes the upfield contact shift for 10,20-H.

(20) Morishima, I.; Kitagawa, S.; Matsuki, E.; Inubushi, T. *J. Am. Chem. Soc.* **1980**, *102*, 2429.

(21) La Mar, G. N.; Walker, F. A. In *The Porphyrins*; Dolphin, D., Ed.; Academic: New York, 1979; Vol. IV, pp 88–89.

(22) Eaton, D. R.; LaLancette, E. A. *J. Chem. Phys.* **1964**, *41*, 3534.

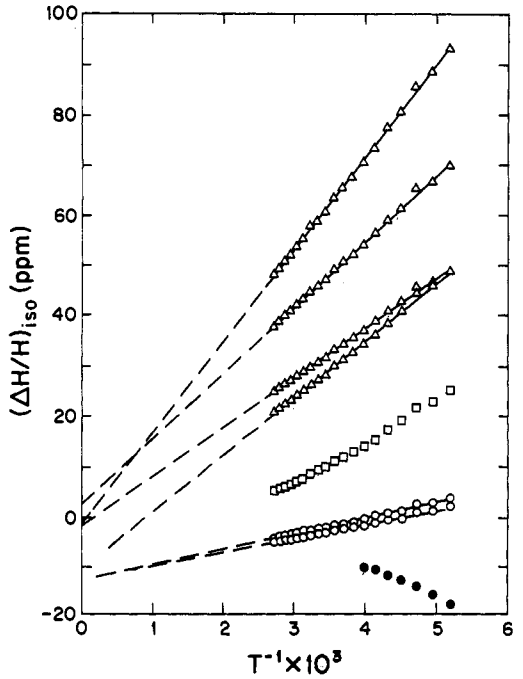

Figure 4. Curie plot for proton resonances of $Fe(OEPBu_2)Cl$ (**2**) in toluene-d_8: (Δ) α-CH_2; (○) β-CH_3; (□) 5,15-H; (●) 52-H.

The temperature dependence of the isotropic shifts have been measured in toluene-d_8 from 193 to 373 K. The Curie plot is illustrated in Figure 4, and a slight curvature is seen for the 5,15-H and 52-H plots. The isotropic shift has two components: the contact shift with a T^{-1} dependence and the dipolar shift with a T^{-2} dependence.[18] Since curvature in a Curie plot should result from a large dipolar shift contribution to the isotropic shift, this is anticipated for 5,15-H, 10,20-H, and 52-H.

$Fe(OEPMe_2)Cl$. The NMR spectrum of **1** is shown in Figure 1, and the pattern is similar to that of **2** although the resonances are substantially broader. Chemical shift assignments proceed as with **2**, albeit with greater uncertainty for 5,15-H and 10,20-H. Chemical shifts, isotropic shifts, and line widths are listed in Table I. Of particular significance is the fact that the 51-H resonance is twice as broad as that of 5,15-H or 10,20-H. For a starting model geometry, we chose the same coordinates as in **2** (40° dihedral roof angle, 12° ruffling angle, 0.40 Å iron displacement, etc.) and experimented with both syn-axial and anti-axial coordination of chloride. Anti-axial coordination of chloride could quickly be eliminated since the calculated value of $\langle L \rangle$ for 51-H was much too small.[23] In fact there is no plausible geometry for anti-axial coordination of chloride that predicts 51-H line widths broader than those of 5,15-H or 10,20-H. The iron atom, displaced 0.40 Å below the coordinating plane, simply would be too distant from the axial methyl groups to explain the observed broadening.

On the other hand, syn-axial coordination of chloride appears certain for the above model geometry, even though this model was developed with structural parameters more appropriate for anti-axial chloride coordination, as in **2**. The calculated metal–proton distances and line-width factors are listed in Table II, and the latter are compared to the experimental line widths. The first feature to notice is that the 51-H resonance is calculated to be approximately twice as broad as the 5,15-H or 10,20-H resonances, as expected for syn-axial chloride coordination. The calculated line-width factor of 51-H is very sensitive to the direction of the 5-C to 51-C bond. In our model this bond is canted outward 8° from a line orthogonal to the tetraaza plane. This opens the cavity between axial methyl groups and allows the chloride to insert with a minimum 51-H to Cl separation of 2.55 Å. In comparison, the crystal structure of **1**, vide infra, shows an outward canting of 6.3° and a 51-H to Cl separation of 2.59 Å. When an axial ligand is not present, however, the methyls are canted inward, 13° for $Ni(OEPMe_2)$ as shown by an X-ray structural analysis,[9] and 12° for $Co(OEPMe_2)$ as deduced from a ^{1}H-NMR line-width factor analysis.[4]

The 5,15-H and 10,20-H resonances are assigned by correspondence with **2**. It is impossible to measure the line width of 10,20-H precisely, even at 500 MHz, since this resonance is sandwiched closely between the 51-H resonance on the left and the solvent resonance on the right. It is estimated to be as broad as the 5,15-H resonance and is so listed in Table I. Our model geometry has 10,20-H more distant from iron than 5,15-H with a smaller line-width factor for the former.

Geometric factors, dipolar shifts, and contact shifts have been calculated for **1**, assuming $D = 15$ cm^{-1}. The numbers are entirely consistent with those listed for **2**. The 51-H proton has a dipolar shift nearly equal to zero because $\langle \theta \rangle$ is close to 54.7°, the value at which $(3\cos^2\theta - 1)/r^3 = 0$. The calculated contact shift for 51-H is 17 ppm, and this is consistent with the anticipated σ delocalization mechanism.

The structure of $Fe(OEPMe_2)Cl$ (**1**) has been solved by single-crystal X-ray diffraction and confirms the assignment of syn-axial chloride coordination as deduced from the ^{1}H NMR line widths.

Atomic coordinates are listed in Table IV, and bond parameters (with estimated standard deviations) are listed in Tables V and VI. The numbering system employed in Tables IV–VI for the carbon and nitrogen atoms in the asymmetric unit of structure

(23) For this model geometry and anti-axial coordination of chloride, the *relative* line width factors are calculated to be 10.0, 10.8, and 7.7 for 5,15-H, 10,20-H, and 51-H, respectively.

Table IV. Fractional Coordinates in the Unit Cell[a]

atom	x	y	z
Fe	0	0.21684 (3)	1/4
Cl	0	0.35693 (7)	1/4
N(1)	0.13728 (14)	0.18796 (4)	0.29069 (14)
N(2)	0.01261 (14)	0.18463 (14)	0.39010 (14)
C(a1)	0.18747 (18)	0.19438 (17)	0.23541 (18)
C(a2)	0.20110 (17)	0.16301 (17)	0.38504 (17)
C(a3)	0.09223 (17)	0.15761 (16)	0.46909 (17)
C(a4)	−0.05248 (18)	0.18930 (16)	0.42717 (17)
C(b1)	0.28150 (18)	0.17444 (18)	0.28981 (19)
C(b2)	0.28921 (18)	0.15521 (17)	0.38331 (19)
C(b3)	0.07207 (19)	0.14462 (17)	0.55282 (18)
C(b4)	−0.01957 (19)	0.16485 (18)	0.52674 (18)
C(5)	0.14777 (18)	0.22162 (19)	0.13017 (19)
C(10)	0.17748 (18)	0.14944 (17)	0.46351 (18)
C(51)	0.15023 (28)	0.31820 (25)	0.12002 (27)
C(11)	0.35621 (21)	0.17384 (25)	0.25090 (25)
C(12)	0.3673 (4)	0.0906 (4)	0.2068 (5)
C(21)	0.37470 (20)	0.12725 (21)	0.46954 (23)
C(22)	0.3788 (3)	0.03375 (29)	0.4839 (4)
C(31)	0.13859 (24)	0.11297 (22)	0.65127 (20)
C(32)	0.1329 (5)	0.02015 (29)	0.6654 (3)
C(41)	−0.07355 (24)	0.16254 (23)	0.,58989 (22)
C(42)	−0.1255 (4)	0.0823 (3)	0.5828 (4)

[a] The estimated standard deviations of the last significant digits are given in parentheses.

Table V. Bond Lengths (Å) in the Coordination Group and Macrocycle Skeleton[a]

Fe–Cl	2.229 (1)	C(a4)–C(b4)	1.410 (3)
Fe–N(1)	2.066 (2)	C(a4)–C(15)	1.501 (4)
Fe–N(2)	2.067 (2)	C(b1)–C(b2)	1.374 (4)
N(1)–C(a1)	1.350 (3)	C(b1)–C(11)	1.505 (4)
N(1)–C(a2)	1.420 (3)	C(b2)–C(21)	1.516 (4)
N(2)–C(a3)	1.407 (3)	C(b3)–C(b4)	1.384 (4)
N(2)–C(a4)	1.346 (3)	C(b3)–C(31)	1.509 (4)
C(a1)–C(b1)	1.422 (4)	C(b4)–C(41)	1.494 (4)
C(a1)–C(5)	1.496 (4)	C(5)–C(51)	1.546 (5)
C(a2)–C(b2)	1.411 (4)	C(11)–C(12)	1.517 (6)
C(a2)–C(10)	1.369 (4)	C(21)–C(22)	1.500 (6)
C(a3)–C(b3)	1.411 (4)	C(31)–C(32)	1.499 (6)
C(a3)–C(10)	1.390 (4)	C(41)–C(42)	1.499 (6)

[a] The number in parentheses following each datum is the estimated standard deviation in the last significant figure.

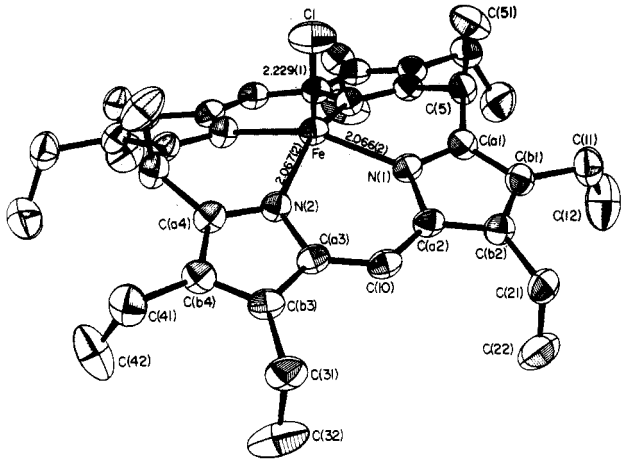

Figure 5. ORTEP diagram (50% ellipsoids) of $Fe(OEPMe_2)Cl$ with listing of Fe–N bond lengths.

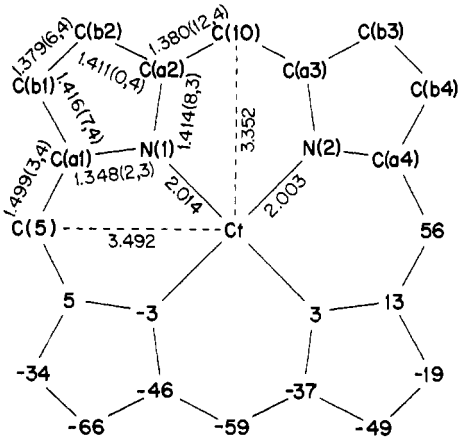

Figure 6. Diagram of the porphodimethene core displaying, on the upper left, the symbols identifying each atom. On the lower half, the atom symbol is replaced by the perpendicular displacement, in units of 0.01 Å, from the mean plane of the four nitrogen atoms of the core. Selected bond distances and the distance of the meso carbon atoms from the center of the four nitrogen atoms (Ct) are shown.

is displayed in Figures 5 and 6. Figure 5 is a computer-drawn model in perspective of the $Fe(OEPMe_2)Cl$ molecule as it exists in the crystal, and the crystallographically imposed twofold axis of symmetry passes through the iron and chlorine atoms. Although not required of the molecule in the crystal, the core of the molecule has approximate C_{2v} symmetry. Figure 6 displays average values of the bond lengths (C_{2v} symmetry) and radii of the core.

The displacement of the skeletal carbon atoms from the mean plane of the four nitrogen atoms is given in Figure 6. In the lower left half of the diagram, the symbol identifying each atom is replaced by the perpendicular displacement (in units of 0.01 Å) of this atom from the mean plane of the four nitrogen atoms. The twofold related atoms in the upper half of the diagram have displacements of the same magnitude and sign. As is usual, local flatness is preserved for each pyrrole ring with the maximum deviation from exact planarity being less than 0.007 Å. As expected, the core is folded along the line joining the two saturated meso carbon atoms (5-C and 15-C of Figure 6). The 34.8° angle between the normals to the pyrromethene halves—the mean plane of a pyrromethene half is defined by atom 15-C and the two unique pyrrole rings—specifies the folding. The two pyrrole rings of a pyrromethene half are almost coplanar; the angle between the normals to the two pyrrole ring mean plane is 3.9°. The comparable values for the folded core of $TiO(OEPMe_2)$ are 38.2 and 4.6°, respectively.

The mean plane of the porphodimethene skeleton is parallel to the mean plane of the four nitrogen atoms but is displaced by 0.19 Å. Consequently, the displacement of individual atoms from the mean plane of the core can be obtained by adding 0.19 Å to the cited displacements given in Figure 6. The iron(III) ion is displaced 0.68 Å out of the mean plane of the porphodimethene core and 0.49 Å out of the plane of the four nitrogen atoms. The conformation of the macrocycle can thus be described as "rooflike" with the two saturated meso carbon atoms, 5-C and 15-C, and the iron(III) ion along the ridge of the roof (Figure 5). The methyl groups of the saturated meso carbon atoms thus have the syn-axial configuration and, along with the chlorine atom, at 1.5 Å above the ridge of the roof occupy what could be termed the chimney positions. The 5-C–51-C bond vectors are canted outward by 6.3° from a vertical position while the corresponding vectors of TiO-$(OEPMe_2)$ are canted inward by 2.6°.[14] The intramolecular contacts between the chlorine atom and the methyl carbon atoms on the saturated meso carbon atoms, Cl···5-C, are 3.651 (5) Å. One of the methyl hydrogens is separated from the chlorine atom by 2.59 (4) Å and deviates from the plane through 15-C, 51-C, Fe, and Cl by 0.09 Å. There are no unusually short intermolecular contacts. The shortest contact is between an atom of the peripheral ethyl groups, 21-C, and one core atom, C(a3), with a distance of 3.527 (4) Å; the others are above 3.6 Å.

It appears now, at least on the basis of three structural determinations, that the fifth group—oxo in $TiO(OEPMe_2)$,[14] nitrido in $MnN(OEPMe_2)$,[24] and chloro in $Fe(OEPMe_2)Cl$—binds preferentially in the syn-axial position. The reason for this preference must be electronic, and not stereochemical, in origin since both coordination sites, top and bottom, are access free. Perhaps the most cogent explanation lies in the nature of the folding of the porphodimethene. When the molecule is folded, the nitrogen lone-pair orbitals are pointed upward and will bind more strongly to iron when it is displaced upward in the direction of the axial methyl groups. A second factor, especially for $Fe(OEPMe_2)Cl$, is the electrostatic interaction between the chloride ligand and 51-H. The chloride is sandwiched between the axial methyl groups with a closest Cl–H approach of 2.59 Å. For $TiO(OEMPe_2)$[14] and $MnN(OEPMe_2)$,[24] this second effect is less important because the axial ligands are nestled below the methyl groups due to the short Ti=O and Mn≡N bonds, respectively.

Table VI. Bond Angles (deg) in the Coordination Group and Macrocycle Skeleton[a,b]

ClFeN(1)	102.85 (6)	N(2)C(a4)C(15)	123.3 (2)
ClFeN(2)	104.35 (6)	C(b4)C(a4)C(15)	124.1 (2)
N(1)FeN(1)′	154.30 (13)	C(a1)C(b1)C(b2)	106.2 (2)
N(2)FeN(2)′	151.29 (12)	C(a1)C(b1)C(11)	126.2 (3)
N(1)FeN(2)	88.68 (8)	C(b2)C(b1)C(11)	127.7 (3)
N(1)FeN(2)′	84.99 (8)	C(a2)C(b2)C(b1)	107.6 (2)
C(a1)N(1)C(a2)	104.8 (2)	C(a2)C(b2)C(21)	124.9 (3)
C(a1)N(1)Fe	127.5 (2)	C(b1)C(b2)C(21)	127.5 (3)
C(a2)N(1)Fe	127.5 (2)	C(a3)C(b3)C(b4)	107.2 (2)
C(a3)N(2)C(a4)	104.9 (2)	C(a3)C(b3)C(31)	125.7 (3)
C(a3)N(2)Fe	127.6 (2)	C(b4)C(b3)C(31)	127.1 (3)
C(a4)N(2)Fe	127.4 (2)	C(a4)C(b4)C(b3)	105.7 (2)
N(1)C(a1)C(b1)	112.0 (2)	C(a4)C(b4)C(41)	126.4 (3)
N(1)C(a1)C(5)	123.1 (2)	C(b3)C(b4)C(41)	127.9 (2)
C(b1)C(a1)C(5)	124.9 (2)	C(a1)C(5)C(a4)′	114.0 (2)
N(1)C(a2)C(b2)	109.4 (2)	C(a1)C(5)C(51)	111.9 (3)
N(1)C(a2)C(10)	123.5 (2)	C(a4)′C(5)C(51)	110.1 (3)
C(b2)C(a2)C(10)	127.1 (2)	C(a2)C(10)C(a3)	129.1 (2)
N(2)C(a3)C(b3)	109.6 (2)	C(b1)C(11)C(12)	114.3 (3)
N(2)C(a3)C(10)	123.5 (27)	C(b2)C(21)C(22)	112.6 (3)
C(b3)C(a3)C(10)	126.8 (2)	C(b3)C(31)C(32)	114.0 (3)
N(2)C(a4)C(b4)	112.5 (2)	C(b4)C(41)C(42)	114.2 (3)

[a] The number in parentheses following each datum is the estimated standard deviation in the last significant figure. [b] Primed and unprimed symbols denote a pair of atoms related by the twofold axis. C(5) and C(15) are also related by the twofold axis.

Acknowledgment. Financial support of the following institutions is gratefully acknowledged: Deutsche Forschungsgemeinschaft, Fonds der Chemischen Industrie, Vereinigung von Freunden der Technischen Hochschule Darmstadt, Darmstadt, West Germany,

(24) Buchler, J. W.; Dreher, C.; Lay, K. L.; Lee, Y. J. A.; Scheidt, W. R. *Inorg. Chem.* **1983**, *22*, 888.

the National Institutes of Health (Grant GM 38401), and NATO (Grant 0034/85). We thank Professor D. N. Hendrickson (University of Illinois) for the computer simulation of the magnetic susceptibility data, Professor W. Haase and Dr. H. Astheimer (Institut für Physikalische Chemie, THD) for the magnetic susceptibility measurements, and Erik Shankland (University of Washington) for running some of the NMR spectra.

Supplementary Material Available: Listing of the anisotropic thermal parameters (1 page); tables of calculated and observed structure factors (9 pages). Ordering information is given on any current masthead page.

Contribution from the Kenan Laboratories of Chemistry,
The University of North Carolina, Chapel Hill, North Carolina 27514

Observations on the Composition of Prussian Blue Films and Their Electrochemistry

C. A. Lundgren and Royce W. Murray*

Received September 1, 1987

Cyclic voltammetric, energy dispersive X-ray analysis, XPS, ferric equivalent weight, and spectroelectrochemical observations have been made of Prussian blue films grown on Pt and SnO_2 electrodes, aiming at an improved picture of the composition and electrochemical reactions of the ferric ferrocyanide films. EDX shows that as-grown films contain no alkali-metal cation and a chloride impurity, similar to results reported for the single-crystal insoluble form Prussian blue by Ludi et al. The film's composition is altered, however, to an alkali-metal content intermediate between those of insoluble and soluble form Prussian blue, upon cyclical electrochemical reduction of the film's ferric states. Ferric sites are lost, and some alkali-metal cation is incorporated into the film. A compositional model is drawn on the basis of analytical and ferric equivalent weight results. Behavior of the films during voltammetric oxidation is consistent with the model, and no electrolyte anion dependencies on the redox potentials are found. Two different kinds of ferric sites are expected on the basis of the observation that the film has a partly insoluble form composition. These two sites are detected in three ways, by splitting of the voltammetric peak in K^+ and NH_4^+ electrolytes, by spectral observation in KCl that two absorbance changes occur that correlate with the potentials of voltammetric peaks, and by previous observations by Feldman and Murray that the films in alkali-metal and ammonium electrolytes exhibit two ferric states with differing electron self-exchange rates as well as differing potentials in alkali-metal and ammonium electrolytes.

Interest in ferric ferrocyanide (Prussian blue, Fe(III/II)), an important member of the family of metal hexacyanometalates,[1] was renewed several years ago by the development of procedures[2,3] for coating it as films on electrodes. Electrochemical reactions of the mixed-valent coatings gave new insights into Prussian blue electron-transfer chemistry[4] and spectroscopy.[5] This research and analogous cyanometalate work by Bocarsly et al.[6] and Crumbliss et al.[7] has recently been reviewed.[8]

Prussian blue has been described in two formulations, the "soluble" form, $KFe^{III}[Fe^{II}(CN)_6]$, and the "insoluble" form, $Fe^{III}_4[Fe^{II}(CN)_6]_3 \cdot 6H_2O$, with the common names having historical peptization rather than actual solubility connotations. Keggin and Miles[9] suggested for the soluble form a face-centered cubic lattice structure in which the high-spin ferric and low-spin ferrocyanide sites are each octahedrally surrounded by –NC and –CN units, respectively, with the K^+ counterion being in an interstitial site. The insoluble Prussian blue structure described in the single crystal study by Ludi et al.[10,11] is also a (primitive) cubic lattice, but one-fourth of the $Fe^{II}(CN)_6$ units are missing, with their nitrogen sites occupied instead by water molecules coordinated to Fe(III) sites and with as many as eight additional water molecules located interstitially.

It has turned out that uncertainties about which of these two stoichiometries of Prussian blue films (if either) represent the films on electrodes have hampered interpretation of the electrochemical studies.[8] The ferric/ferrous reduction reaction for Prussian blue coatings is written by Neff et al.[12] as of the soluble form

$$KFe^{III}[Fe^{II}(CN)_6] + e^- + K^+ \rightarrow K_2Fe^{II}[Fe^{II}(CN)_6] \quad (1)$$

and by Itaya et al.[5] as of the insoluble form

$$Fe^{III}_4[Fe^{II}(CN)_6]_3 \cdot 6H_2O + 4e^- + 4K^+ \rightarrow K_4Fe^{II}_4[Fe^{II}(CN)_6]_3 \cdot 6H_2O \quad (2)$$

Both reduction reactions require, for electroneutrality, entry of K^+ (or another appropriately sized electrolyte cation) into the lattice, and experimental results confirm such a cation dependency.[5,12,13]

The ferrocyanide/ferricyanide oxidation reactions are also written differently, as[12]

$$3KFe^{III}[Fe^{II}(CN)_6] - 2e^- - 2K^+ \rightarrow KFe^{III}_3[Fe^{III}(CN)_6]_2[Fe^{II}(CN)_6] \quad (3)$$

where part of the lattice K^+ departs from the lattice and the oxidative charge is two-thirds of the reductive charge, and as[5]

$$Fe^{III}_4[Fe^{II}(CN)_6]_3 \cdot 6H_2O - 3e^- + 3X^- \rightarrow Fe^{III}_4[Fe^{II}(CN)_6]_3(X)_3 \cdot 6H_2O \quad (4)$$

where an electrolyte anion enters the lattice and the oxidative charge is three-fourths of the reductive charge. The reported[5] charge ratio, 0.71, is an indecisively intermediate value. Analyses by Itaya et al.[5] show as-grown Prussian blue films contain no K^+, which is inconsistent with the soluble formulation, but on the other hand, the soluble formulation of reaction 3 is favored by shifts of the potentials of the electrochemical waves with electrolyte concentration,[12] mass *loss* data,[13] and comparative insensitivity to electrolyte anion identity.[12,13]

We originally became interested in using Prussian blue in a bilayer electrode[14] and as an object of a electron-hopping kinetics study,[15] since it is an ostensibly internally ordered electroactive material. In view of the previous uncertainties about the composition of the electrode coatings, we mounted the analytical,

(1) Sharp, A. G. *The Chemistry of Cyano Complexes of the Transition Metals*; Academic: London, 1976; pp 121–126.
(2) Neff, V. K. *J. Electrochem. Soc.* **1978**, *125*, 886.
(3) Itaya, K.; Akahoshi, H.; Toshima, S. *J. Electrochem. Soc.* **1982**, *129*, 1498.
(4) Rajan, K.; Neff, V. D. *J. Phys. Chem.* **1982**, *86*, 4361.
(5) Itaya, K.; Ataka, T.; Toshima, S. *J. Am. Chem. Soc.* **1982**, *104*, 4767.
(6) Sinha, S.; Humphrey, B. D.; Bocarsly, A. B. *Inorg. Chem.* **1984**, *23*, 203.
(7) Crumbliss, A. L.; Lugg, P. S.; Morosoff, N. *Inorg. Chem.* **1984**, *23*, 4701.
(8) Itaya, K.; Uchida, I.; Neff, V. D. *Acc. Chem. Res.* **1986**, *19*, 162.
(9) Keggin, J. F.; Miles, F. D. *Nature (London)* **1936**, *137*, 577.
(10) Buser, H. J.; Schwarzenbach, D.; Petter, W.; Ludi, A. *Inorg. Chem.* **1977**, *16*, 2704.
(11) Herren, F.; Fischer, P.; Ludi, A.; Halg, W. *Inorg. Chem.* **1980**, *19*, 956.
(12) Ellis, D.; Eckhoff, M.; Neff, V. D. *J. Phys. Chem.* **1981**, *85*, 1225.
(13) Feldman, B. J.; Melroy, O. R., submitted for publication in *J. Electroanal. Chem.* Interfacial Electrochem.
(14) Abruna, H. D.; Denisevich, P.; Umana, M.; Meyer, T. J.; Murray, R. W. *J. Am. Chem. Soc.* **1981**, *103*, 1.
(15) Feldman, B. J.; Murray, R. W. *Inorg. Chem.* **1987**, *26*, 1702.

0020-1669/88/1327-0933$01.50/0